

Optimization of 3x3 neuromorphic photonic network for programmable Boolean operations

*Original*

Optimization of 3x3 neuromorphic photonic network for programmable Boolean operations / Marchisio, Andrea; Cem, Ali; Ding, Yunhong; Curri, Vittorio; Carena, Andrea; Da Ros, Francesco; Bardella, Paolo. - ELETTRONICO. - 12880:(2024). (Intervento presentato al convegno SPIE Photonic West tenutosi a San Francisco, CA, USA nel 27 January - 1 February 2024) [10.1117/12.3002953].

*Availability:*

This version is available at: 11583/2986949 since: 2024-03-13T14:42:43Z

*Publisher:*

SPIE

*Published*

DOI:10.1117/12.3002953

*Terms of use:*

This article is made available under terms and conditions as specified in the corresponding bibliographic description in the repository

*Publisher copyright*

SPIE postprint/Author's Accepted Manuscript e/o postprint versione editoriale/Version of Record con

Copyright 2024 Society of PhotoOptical Instrumentation Engineers (SPIE). One print or electronic copy may be made for personal use only. Systematic reproduction and distribution, duplication of any material in this publication for a fee or for commercial purposes, and modification of the contents of the publication are prohibited.

(Article begins on next page)

# Optimization of 3×3 neuromorphic photonic network for programmable Boolean operations

Andrea Marchisio<sup>a</sup>, Ali Cem<sup>b</sup>, Yunhong Ding<sup>b</sup>, Vittorio Curri<sup>a</sup>, Andrea Carena<sup>a</sup>,  
Francesco Da Ros<sup>b</sup>, and Paolo Bardella<sup>a</sup>

<sup>a</sup>Department of Electronics and Communications, Politecnico di Torino, Turin, Italy

<sup>b</sup>Department of Electrical and Photonics Engineering, Technical University of Denmark,  
Denmark

## ABSTRACT

We propose a methodology to analyze a 3×3 Mach-Zehnder-based neuromorphic optical network used as a programmable logic gate. The investigated approach starts from the electromagnetic simulation of the integrated optical elements, then moves to the description of the thermal heaters including thermal cross-talk, and finally addresses the definition of the logical levels.

**Keywords:** Neuromorphic Circuit, Photonic Integrated Circuit, Numerical Modeling

## 1. INTRODUCTION

The use of neuromorphic silicon photonic circuits represents a significant advance in the realm of artificial intelligence. These circuits can accurately process information in the optical domain, with processing speeds and energy consumption that are potentially much better than their electrical counterpart.<sup>1,2</sup> In addition, the possibility to integrate these circuits into classical silicon platforms used by traditional electronics fabrication processes and the programmability offered by these solutions represent two relevant advantages of these technologies.

It is important to note that the number of components in Photonic Integrated Circuits (PICs) has grown consistently in recent decades.<sup>3</sup> As a consequence, the design and analysis of these devices are becoming increasingly challenging, and the measured behavior of the circuit can deviate significantly from the expected behavior. Among the main causes of these discrepancies are fabrication tolerances and tuning problems.<sup>4</sup> To develop suitable models for the control of these PICs, it is particularly important to properly describe the various components, not only as isolated elements but also considering thermal and electrical crosstalk properly, which could significantly degrade overall performance.<sup>5-8</sup>

In the following, we describe the analysis of a 3×3 neuromorphic network, starting from the electromagnetic simulations, then taking into account thermal effects, and finally performing a system simulation. Finally, an approach to identify the threshold to apply when using the device as a logical gate is presented.

## 2. REFERENCE DEVICE

The considered device consists of nine interconnected Mach-Zehnder interferometers (MZIs), with a total of three input ports and three output ports, as shown in Fig. 1. The output powers are linear combinations of the input signals, dynamically weighted by the thermally tuneable MZIs, based on two 2×2 Multi-Mode Interferometers (MMIs). Four optical crossings are also present.

The device is designed for operation in the C-band and is part of a larger, 7×7 Photonic Integrated Circuit (PIC) designed in the Department of Photonics Engineering of the Technical University of Denmark (DTU)<sup>9,10</sup> as a reconfigurable optical switch. The PIC is designed on a silicon-on-insulator (SOI) platform with a top silicon thickness of 250 nm and a straight waveguide width of 250 nm, and was manufactured by a single step of standard SOI processing, including e-beam lithography and Inductively Coupled Plasma (ICP) etching, followed by additional steps of lithography and metal liftoff for the fabrication of the metallic heater on the upper branch

---

Send correspondence to [paolo.bardella@polito.it](mailto:paolo.bardella@polito.it)

of each MZI. These heaters act as Thermo-Optical Phase Shifters (TOPS) and consist of a resistive titanium region, with  $0.1\text{ }\mu\text{m}$  thickness,  $1.8\text{ }\mu\text{m}$  width and  $10\text{ }\mu\text{m}$  length, placed on top of the waveguide separated by an oxide layer.<sup>11</sup>

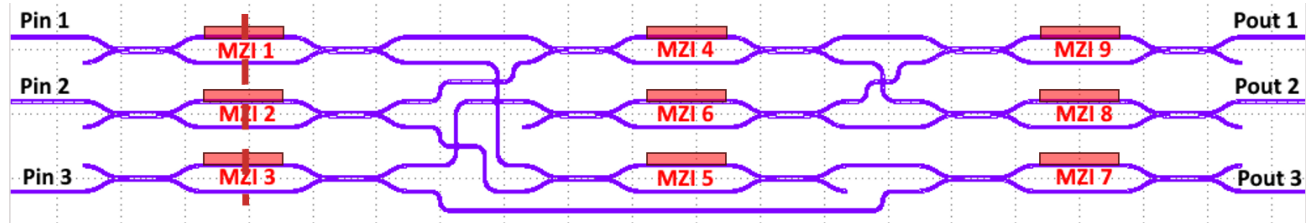


Figure 1. Schematic of the  $3\times 3$  considered circuit. Labels M1–M9 identify the nine MZIs. The overall dimension is approximately  $1800\text{ }\mu\text{m}\times 250\text{ }\mu\text{m}$ . The red dashed line indicates the position of the cross-section thermal distribution shown in Fig. 3.

### 3. FDTD SIMULATIONS

In order to gain more insight into MZIs and crossings, we used Finite Differences Time-Domain simulations in Synopsys RSoft<sup>®</sup> to analyze these components and extract the optical losses associated with each fundamental block. The distribution of optical power at the MZI output ports as a function of the variation of the refractive index in one of its branches is also investigated. An example of the analyzes we performed is shown in Fig. 2.

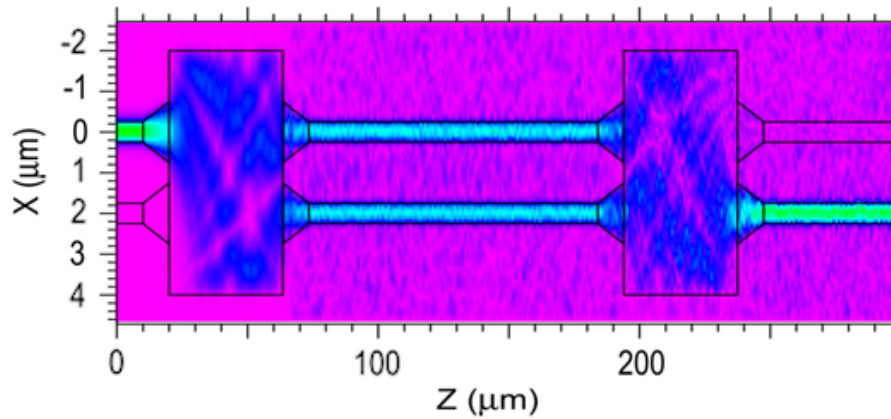


Figure 2. Example of FDTD simulations of the MZI.

### 4. THERMAL SIMULATIONS

The tuning of the MZIs is obtained thanks to the TOPS: numerical simulations are required to correlate the applied voltage to heat and to the corresponding variation of the refractive index, and to quantify the strength of thermal crosstalk between adjacent MZIs.

For the goals of this analysis, we use COMSOL Multiphysics and consider a 3D representation of a section of the device containing three vertically adjacent MZIs (such as MZI 1, 2, and 3 in Fig. 1), the horizontal separation between MZIs being sufficiently large to ignore any thermal effect. An example of simulation results is presented in Fig. 3, where a voltage of  $2\text{ V}$  is applied to the electrode of MZI 2: as a result, the temperature in the underlying waveguide is heated to  $70.7\text{ }^{\circ}\text{C}$ , but the temperature of the second waveguide of MZI 1 is also increased by  $5\text{ }^{\circ}\text{C}$  with respect to the other branch, even if no voltage is applied to the corresponding heater. This thermal crosstalk represents an important effect for proper control of the device. Thanks to these simulations, we were able to map the voltages applied to the three MZIs into variations of refractive indices in the six waveguides and obtain a complete picture of the whole device tuning.

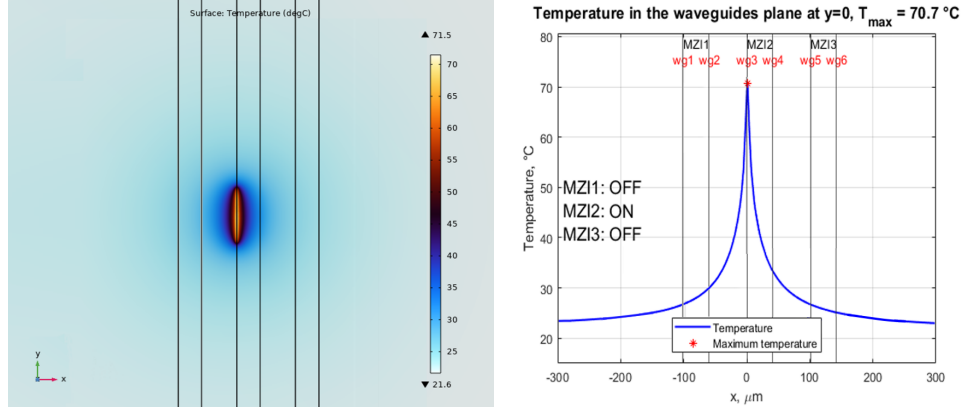


Figure 3. Top view (left) and cross section of the temperature distribution in the position indicated by the red line in Fig. 1 (right), at the waveguides height, when a 2 V control voltage is applied to the heater of MZI 2. The vertical lines indicate the positions of the waveguides.

## 5. SYSTEM LEVEL SIMULATIONS

The calculation of the powers at the three output ports as functions of the control voltages and the powers at the three input port is straightforward: the device does not contain closed loops and the power  $P_{out,u}^k$  at the output of the upper branch of MZI  $k$  can be simply calculated as a linear combination of the powers  $P_{in,u}^k$  and  $P_{in,l}^k$  at its two input ports:

$$\chi = s_1 + s_2 \sin^2(\theta_k + \phi_k)$$

$$P_{out,u}^k = (1 - \alpha)(P_{in,u}^k \chi + P_{in,l}^k (1 - \chi))$$

with  $\alpha$  optical losses of the MZI,  $s_1$  and  $s_2$  split coefficients taking into account the non complete transfer of power from the two MZI branches, obtained from FDTD simulations;  $\theta_k$  is a phase term which depends on the voltages applied to MZI  $k$  and its adjacent ones, and is extracted from thermal simulations. Finally,  $\phi_k$  is an additional phase term that takes into account non-ideal behaviors of the single MZI.

The results of the model are then compared to the experimental measurements performed at DTU. To better understand the individual behavior of each MZI, in the experimental setup all MZI electrodes are grounded, except for one electrode at the time, whose voltage is tuned between 0 V and 2 V, approximately corresponding to a shift between 0° and 180°. An input signal is injected at port 1 and the output is measured at port 2: In this configuration, MZI 2 should have no effect since no signal is injected at port 2, but a change in the voltage of this MZI causes a change in the phase of MZI 1 due to thermal crosstalk. Figure 4 shows a comparison between measurements and simulations: The model is capable of reproducing the role of MZI 2, successfully including thermal crosstalk. The remaining discrepancies are supposedly caused by other crosstalk effects, such as unwanted transfer of signal between the circuit electrical paths, which all share the same ground connection.

## 6. THRESHOLDS FOR OPERATION AS BOOLEAN GATE

The control voltages of the MZIs can be selected to implement up to three Boolean functions of the signal at the input ports. In this scenario, the input powers are assumed to be logical quantities representing a false (null power) or true (non-null power) value. The value of the power corresponding to the true level is not significant for this analysis, since we assume that the level is so low to allow us to neglect non-linear effects such as Two-Photon Absorption.<sup>12</sup> However, while input signals are considered to be either 0 or 1, we need to calculate which is the distribution of the values at the output ports as functions of the control voltages. For this reason, 50 000 simulations were performed with random values of the nine control voltages ranging from 0 V to 2 V and for the  $2^3 = 8$  combinations of the Boolean input powers. We obtained as a result the distribution of the powers at each output port, from which we extracted the median value, then used as a threshold to distinguish between false

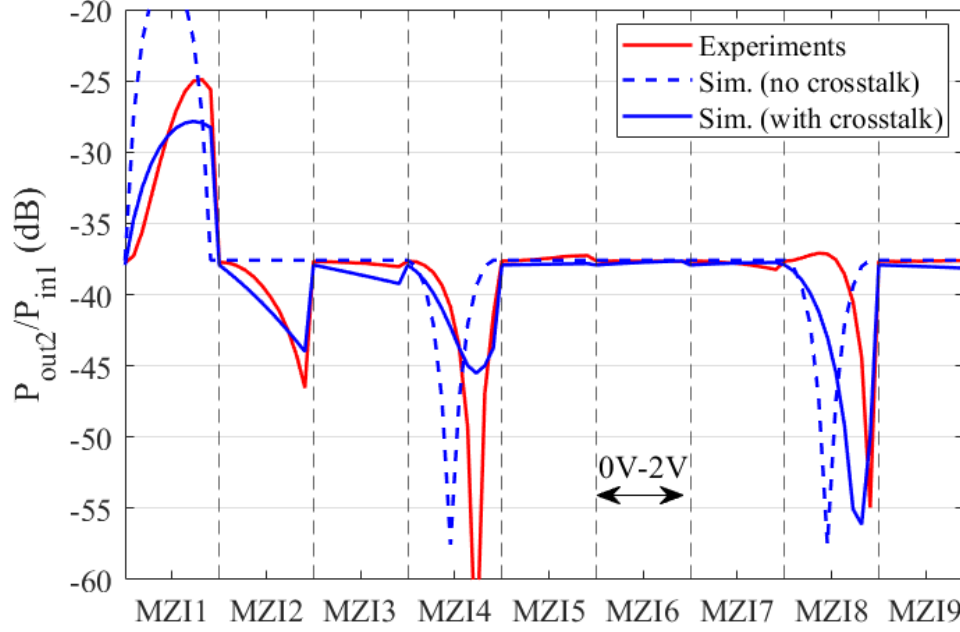


Figure 4. Power at output port 2 with input signal at port 1, as a function of the MZIs' voltages: experiments (red), simulation without crosstalk (dashed blue), and simulation including crosstalk (blue). In each interval delimited by vertical dashed lines, the voltage of one MZI is tuned 0 V and 2 V, while the other MZIs are grounded.

and true output values. For the considered device, the thresholds of the three ports are 0.076, 0.046 and 0.093, respectively.

Once the thresholds have been identified, we can use an optimization algorithm, such as the Particle Swarm Optimization method, to determine the optimal values of the control signals to obtain the logic function requested by the user at a certain port.

## 7. CONCLUSIONS

A methodology for modeling thermal crosstalk in integrated photonic circuits was discussed. We analyzed a  $3 \times 3$  programmable optical circuit and, after FDTD simulations of the fundamental components, we then continued with a thermal analysis of the area beneath the heaters. The findings of these analyzes were then used to perform a system-level simulation of the device, resulting in reasonably accurate predictions of the experimental findings. We finally identified the logical thresholds corresponding to the true or false levels at the output.

## REFERENCES

- [1] E. Srouji *et al.*, "Photonic and optoelectronic neuromorphic computing," *APL Photonics*, vol. 7, no. 5, p. 051101, 05 2022.
- [2] B. J. Shastri *et al.*, "Photonics for artificial intelligence and neuromorphic computing," *Nat. Photonics*, vol. 15, no. 2, pp. 102–114, Feb 2021.
- [3] N. Margalit *et al.*, "Perspective on the future of silicon photonics and electronics," *Applied Physics Letters*, vol. 118, p. 220501, 05 2021.
- [4] M. Y.-S. Fang *et al.*, "Design of optical neural networks with component imprecisions," *Opt. Express*, vol. 27, no. 10, pp. 14 009–14 029, 2019.
- [5] S. Biasi *et al.*, "On the effect of the thermal cross-talk in a photonic feed-forward neural network based on silicon microresonators," *Frontiers in Physics*, vol. 10, 2022.
- [6] S. Bandyopadhyay *et al.*, "Hardware error correction for programmable photonics," *Optica*, vol. 8, no. 10, pp. 1247–1255, Oct 2021.

- [7] L. Tunesi *et al.*, “Thermal control scheme in contra-directional couplers for centered tunable bandwidths,” in *2023 International Conference on Numerical Simulation of Optoelectronic Devices (NUSOD)*, 2023, p. 115 – 116.
- [8] M. Orlandin *et al.*, “Thermal crosstalk effects in a silicon photonics neuromorphic network,” in *2023 International Conference on Numerical Simulation of Optoelectronic Devices (NUSOD)*, 2023, p. 43 – 44.
- [9] M. A. Nahmias *et al.*, “Photonic multiply-accumulate operations for neural networks,” *IEEE J. Sel. Top. in Quantum Electron.*, vol. 26, no. 1, pp. 1–18, 2020.
- [10] L. De Marinis *et al.*, “Photonic integrated reconfigurable linear processors as neural network accelerators,” *Appl. Sci.*, vol. 11, no. 13, 2021.
- [11] Y. Ding *et al.*, “Reconfigurable sdm switching using novel silicon photonic integrated circuit,” *Sci. Rep.*, vol. 6, no. 1, p. 39058, Dec 2016.
- [12] A. D. Bristow *et al.*, “Two-photon absorption and Kerr coefficients of silicon for 850–2200nm,” *APL*, vol. 90, no. 19, p. 191104, 05 2007.